Sound Insulation Performance of Acoustic Metamaterials Based on Attachable Helmholtz Resonators

ZUO Hongwei[1,2], *LI Jinze*[3], *SHEN Cheng*[1,2*], *YANG Shasha*[4*], *WANG Bin*[5]

1.State Key Laboratory of Mechanics and Control of Mechanical Structures, Nanjing University of Aeronautics and Astronautics, Nanjing 210016, P. R. China;

2.Nanjing Center for Multifunctional Lightweight Materials and Structures (MLMS), Nanjing University of Aeronautics and Astronautics, Nanjing 210016, P. R. China;

3.Department of Mechanical Engineering, The Hong Kong Polytechnic University, Hong Kong 999077, P. R. China;

4.School of Mechanical Engineering, Nanjing Vocational University of Industry Technology, Nanjing 210023, P. R. China;

5.Suzhou DingYu Energy Saving Equipment Co., Ltd., Suzhou 215213, P. R. China

(Received 22 April 2022; revised 6 July 2022; accepted 21 July 2022)

Abstract: To address the control of low frequency noises, we propose an new perforated thin-plate acoustic metamaterials with the attachable Helmholtz resonator (AHR) which can be directly attached to the existing structure to suppress acoustic radiation. Sound transmission loss of the aluminium plate with AHR has been simulated using the finite element method under a normal incident plane sound wave. The results show that AHR works well in the 50—500 Hz frequency band, with two peaks of insulation occurring and the corresponding frequency of the first insulation peak dropping to around 120 Hz. The study of the effects of plate thickness, cavity depth, perforation radius and perforation length on the sound insulation performance of metamaterials demonstrates that the effective suppression of acoustic radiation at specific frequencies can be achieved by changing the acoustic radiation properties of the structure.

Key words: Helmholtz resonator; acoustic metamaterials; transmission loss

CLC number: TB535 **Document code:** A **Article ID:** 1005-1120(2022)S-0023-09

0 Introduction

With the acceleration of urbanization and the rapid development of the transportation industry, noise pollution has become a serious environmental problem, which greatly affects people's daily life. In order to control the noise, traditional sound insulation materials such as homogeneous panels, laminated panels, etc., have been widely used in construction, transportation, machinery and other fields, but these materials are difficult to solve the problem of low-frequency noise control. According to the mass density law, if traditional sound insulation materials are used, a bulky structure with large surface density is required to effectively attenuate low-frequency sound waves, which is difficult to meet engineering design requirements. In recent years, the emergence of acoustic metamaterials has broken the mass law and opened up new research directions for solving low-frequency noise problems because of their light mass and small size[1-2].

Acoustic metamaterials[3-8] are man-made sub-wavelength composites with negative equivalence parameters, and they can be considered as homogeneous media. By designing microstructures with sub-wavelength dimensions to manipulate sound, researchers have proposed various acoustic metamaterials and applied them to noise reduction, holograms for acoustics, acoustic cloak, etc., achieving excellent acoustic properties such as complete acoustic reflection, perfect acoustic absorption, and

*Corresponding authors, E-mail addresses: cshen@nuaa.edu.cn, 2016100849@niit.edu.cn.

How to cite this article: ZUO Hongwei, LI Jinze, SHEN Cheng, et al. Sound insulation performance of acoustic metamaterials based on attachable Helmholtz resonators[J]. Transactions of Nanjing University of Aeronautics and Astronautics, 2022, 39(S): 23-31.

http://dx.doi.org/10.16356/j.1005-1120.2022.S.004

acoustic focusing[9-14]. To meet the lightweight requirements, the researchers focused on the use of lightweight thin-walled structures to achieve attenuation of low-frequency noise by using films, plates and shells. In 2008, Yang et al.[6] proposed a two-dimensional thin-film acoustic metamaterial that achieved negative mass density and near-total reflection of acoustic waves in the low-frequency range. In 2013, Ma et al.[15] perforated thin-film acoustic metamaterials of additional mass and demonstrated that large transmission loss could still be achieved in the presence of larger orifices for free flow of air. In 2017, Langfeldt et al.[16] improved the design of thin-film acoustic metamaterials by perforating both the mass block and the film and proposed that the perforated structure was able to induce a new anti-resonance before the original first-order natural frequency resulting in a new transmission loss peak at low frequencies. In order to obtain better acoustic performance, coupled structural acoustic metamaterials have been studied. In 2017, Zhou et al.[17] investigated a Helmholtz cavity with a membrane structure, reducing the natural frequency of the original structure and a broadening of the acoustic insulation frequency band. In 2019, He et al.[18] proposed a Helmholtz cavity with thin-film bottom, combining a membrane type acoustic metamaterial and a Helmholtz cavity, which greatly improved the sound insulation performance compared with either structures themselves.

Due to the requirements of weight and space in engineering applications, it is often difficult to avoid the strong near-field coupling effects between panels and objects when inserting panels, resulting in poor sound insulation performance at low frequencies. In this paper, we propose an attachable Helmholtz resonator (AHR) attached to the surface of the structure, which not only induces the anti-phase motion between the structure and mass at the operating frequency, but also excites the vibration of the air at the neck of the cavity, thus effectively attenuating the low-frequency sound waves. Furthermore, the sound insulation performance of AHR attached to the aluminium plate is analyzed by means of theoretical analysis and numerical simulation, and the formation mechanism of transmission loss peaks is analyzed in relation to equivalent parameters and simulated fields. Finally, we investigate the effect of structural dimensions on sound insulation numerically and find that effective control of specific low-frequency noise could be achieved by adjusting the structural parameters of AHR.

1 Attachable Helmholtz Resonators

The unit cell of AHR, shown in Fig.1(a), consists of a circular perforated plate and a cylindrical support frame with a cylindrical perforated mass in the middle of the plate, both having the same aperture. The plate is fixed to the frame, the bottom of which can be attached to the surface of the object that needs to reduce the sound radiation. In the AHR cell, the thickness of the plate is $t_1 = 0.125$ mm and the radius of the plate $r_1 = 10$ mm; the height of the cylindrical mass is $t_2 = 8$ mm and the radius of the cylindrical mass $r_2 = 2$ mm; the thickness of the frame is $t_3 = 1$ mm and the height of the frame $t_4 = 25$ mm. The Young's modulus is $E_1 = 2.5$ GPa, Poisson's ratio $\upsilon_1 = 0.34$ and the density $\rho_1 = 1\,420$ kg/m^3 for the polyimide plate; the Young's modulus is $E_2 = 2.695$ GPa, Poisson's ratio $\upsilon_2 = 0.44$ and the density $\rho_2 = 1\,180$ kg/m^3 for the resin frame; the Young's modulus is $E_3 = 90$ GPa, Poisson's ratio $\upsilon_3 = 0.33$ and the density $\rho_3 = 8\,530$ kg/m^3 for the brass mass. As shown in Fig.1(b), the central perforation of the thin plate and mass, which acts as the neck of the Helmholtz resonator, allows air particles to pass through. When the AHR is attached to

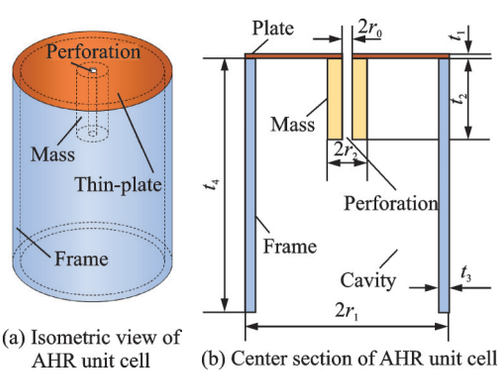

(a) Isometric view of AHR unit cell (b) Center section of AHR unit cell

Fig.1 Geometric model of an AHR unit cell

a closed surface of the object, the frame and the object will form a back cavity, turning the AHR into a Helmholtz resonator with a thin-plate metamaterial on the top surface, which affects the acoustic properties of the object. However, when the AHR is attached to an open surface of the object, it forms a double-opening Helmholtz resonator, which will still affect its acoustic properties without affecting its ventilation[19]. In order to investigate the acoustic properties of AHR, we take an aluminium plate of thickness $t_4 = 1$ mm as the backing plate and investigate the effect of AHR on the acoustic properties of the aluminium plate.

1.1 Equivalent models

The Helmholtz resonator, shown in Fig.2(a), has a rigid cavity with an open cross-sectional area of S_h, a neck length of l_h, and a cavity volume of V_h.

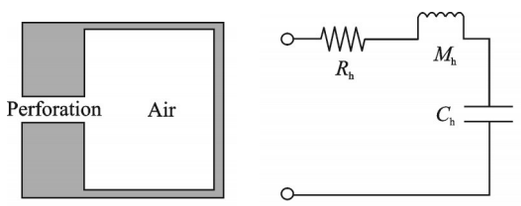

(a) Geometric model of the Helmholtz resonator (b) Equivalent circuit model of the Helmholtz resonator

Fig.2 Geometric model and equivalent circuit model of the Helmholtz resonator

As the acoustic radiation from the perforation increases the equivalent length of the cavity neck, the corrected cavity neck length, taking into account the end effect, is $l_{eff} = l_h + 1.7r_0$, where r_0 is the radius of the perforation.

The Helmholtz resonator can be transformed into an equivalent circuit model, as shown in Fig.2(b), which consists of acoustic mass M_h, acoustic capacitance C_h, acoustic resistance R_h and the resonant frequency f_h can be described as

$$f_h = \frac{1}{2\pi}\sqrt{\frac{1}{M_h C_h}} \tag{1}$$

where

$$M_h = \frac{V_h}{\rho_0 c_0^2} \tag{2}$$

$$C_h = \frac{\rho_0 l_{eff}}{S_h} \tag{3}$$

The first-order resonance frequency of a circular plate is

$$f_p = \frac{\mu^2 h_p}{4\pi r_p^2}\sqrt{\frac{E_p}{3\rho_p(1-\sigma_p^2)}} \tag{4}$$

where $\mu = 3.20$, h_p is the thickness of the plate, E_p the Young's modulus of the plate, ρ_p the density of the plate, r_p the radius of the plate, and σ_p the Poisson's ratio. The equivalent mechanical mass M_F can be found as

$$M_F = 2m_p J_0^2(\mu) \tag{5}$$

where $m_p = \pi r_p^2 h_p \rho_p$ is the actual mass of the circular plate and J_0 the zero-order Bessel function.

The first-order resonant mode of the circular plate structure is a symmetric vibration, which can be considered as a "spring-vibrator" system with an equivalent stiffness K_F. The resonant frequency of this structure can also be expressed as

$$f_p = \frac{\sqrt{K_F/M_F}}{2\pi} \tag{6}$$

Set $\omega_p = 2\pi f_p$, then

$$K_F = 2m_p \omega_p^2 J_0^2(\mu) \tag{7}$$

A mass unit m_{add} is attached to the center of the circular plate, as shown in Fig.3(a). Since the first-order resonant mode of the circular plate-mass structure is a symmetric vibration, it can still be considered as a "spring-vibrator" system, and the equivalent mass of the model M_F becomes

$$M_F' = 2m_p J_0^2(\mu) + m_{add} \tag{8}$$

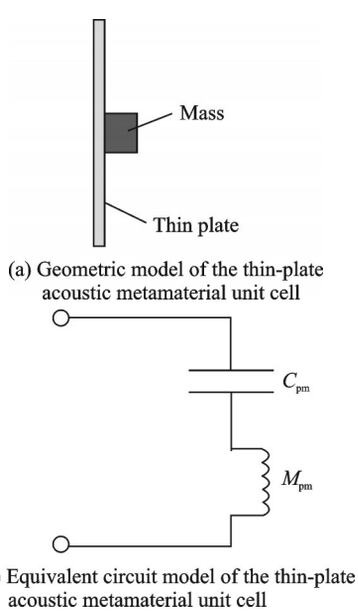

(a) Geometric model of the thin-plate acoustic metamaterial unit cell

(b) Equivalent circuit model of the thin-plate acoustic metamaterial unit cell

Fig.3 Geometric model and equivalent circuit model of the thin-plate acoustic metamaterial unit cell

The resonant frequency of this system f_{pm} becomes

$$f_{pm}=\frac{\sqrt{K_F/M_F'}}{2\pi} \tag{9}$$

Set $\omega_{pm}=2\pi f_{pm}$. Since the circular plate is fixed all around, the equivalent area of the force-acoustic transducer is $S_{eff}=0.309S_p$, where S_p is the area of the thin plate. As shown in Fig.3(b), the thin-plate acoustic metamaterial is transformed into an equivalent circuit model, where the acoustic mass M_{pm} and the acoustic capacitance C_{pm} of the structure are

$$M_{pm}=\frac{2m_pJ_0^2(\mu)+m_{add}}{0.309^2S_p^2} \tag{10}$$

$$C_{pm}=\frac{0.309^2S_p^2}{2m_p\omega_{pm}^2J_0^2(\mu)} \tag{11}$$

1.2 Derivation of effective parameters

Since the thin-plate acoustic metamaterial is sub-wavelength in size, i.e. the incident acoustic wave wavelength is much greater than the thickness of the metamaterial, the metamaterial can be regarded as homogeneous and its effective parameters can be calculated from the sound transmission coefficient T and the sound reflection coefficient R. The thickness of the structure studied in this paper is $t<$ 60 mm and the speed of sound in air is known to be c=343 m/s, so when the frequency of the incident acoustic wave is below 500 Hz, the acoustic wave wavelength will be greater than 686 mm, satisfying the sub-wavelength condition.

When a plane wave is incident on a homogeneous liquid acoustic layer from a fluid medium, according to the retrieval method[20], the reflection and the transmission coefficient are

$$R=\frac{Z_1^2-Z_0^2}{Z_0^2+Z_1^2+2\mathrm{i}Z_0Z_1\cot\phi} \tag{12}$$

$$T=\frac{1+R}{\cos\phi-\dfrac{Z_1\mathrm{i}\sin\phi}{Z_0}} \tag{13}$$

where $Z_0=\rho_0c_0$, $Z_1=\rho_1c_1$ are the impedance of the fluid medium and the homogeneous layer, respectively; ρ_0, c_0 the density and the sound speed of the fluid medium, respectively; and ρ_1, c_1 the density and the sound speed of the homogeneous layer, respectively. ϕ is the phase change of the sound wave after passing through the homogeneous layer. Introducing the acoustic impedance $\xi=\rho_1c_1/(\rho_0c_0)$, the refractive index $n=c_0/c_1$, the following relationship can be obtained

$$\xi=\frac{r}{1-2R+R^2-T^2} \tag{14}$$

$$n=\frac{-\mathrm{i}\ln x+2\pi m}{kd} \tag{15}$$

where

$$r=\mp\sqrt{(R^2-T^2-1)^2-4T^2} \tag{16}$$

$$x=\frac{1-R^2+T^2+r}{2T} \tag{17}$$

and ρ_1 is the wave vector and d the thickness of the homogeneous layer. The effective mass density ρ_{eff} and the effective bulk modulus K_{eff} of the homogeneous layer can be found from ξ and n, shown as

$$\rho_{eff}=\rho_0n\xi \tag{18}$$

$$K_{eff}=K_0\xi/n \tag{19}$$

where K_0 is the bulk modulus of the fluid medium.

1.3 Simulation and calculation

We use COMSOL multiphysics software to calculate the natural frequencies, sound transmission loss and effective parameters. For the model used in simulation, the radius of backplate is r_4= 49.5 mm and the radius of perforation r_0=0.5 mm. In the numerical simulation, the incident sound wave is a simple harmonic plane wave with an amplitude of 1 Pa, which is incident perpendicularly on the sample with frequency swept over interested ranges. The horizontal boundary of the backplate is set to be fixed. The upstream and downstream air domains are connected to the front and rear surfaces of the plate, respectively, and the end surfaces of the air domains are set as absorbing boundaries. The transmission loss can be calculated using TL= $10\lg(W_{in}/W_{out})$, where W_{in} and W_{out} are the incident and transmitted acoustic energy, respectively.

Fig.4 shows the sound transmission loss lines, where the solid line shows the simulation results for the original aluminium plate and the short line shows the simulation results for the aluminium plate with AHR. It can be seen that in the low frequency range of 50—500 Hz, the aluminium plate with AHR has two additional peaks of the sound insula-

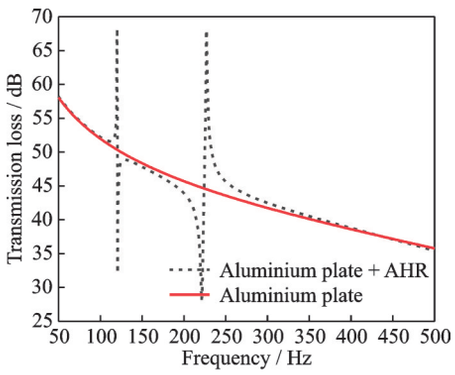

Fig.4 Comparison of calculated sound transmission loss curves for the original aluminium plate and the aluminium plate with AHR attached

tion compared with the original aluminium plate, and that in the frequency range of 90—120 Hz and 225—440 Hz the aluminium plate with AHR has a significant increase in the sound insulation performance. Both sound insulation peak values are more than 15 dB higher than the transmission loss of the original aluminium plate. In detail, the first insulation peak occurs at 119.9 Hz with a transmission loss of 68.3 dB and the second insulation peak occurs at 227.0 Hz with a transmission loss of 68.0 dB. As is evident from the previous section, the resonant frequencies of the thin plate mass structure and the ideal Helmholtz cavity of this size can be calculated as 109.3 Hz and 205.5 Hz, respectively. There is a certain difference between the result and the peak frequency of the sound insulation calculated by the simulation. The main reasons are that the equivalent stiffness of the thin plate with mass attachment is replaced by the equivalent stiffness of the thin plate without the mass attachment, the effect of perforation on the equivalent stiffness of the thin plate is not considered, and the assumption that the Helmholtz cavity is integrally rigid. In reality, however, the mass base fixes a portion of the plate, causing the equivalent modulus to change; the perforation changes the boundary conditions and the equivalent modulus of the plate; the AHR is not absolutely rigid; and the combination of the mass plate and the Helmholtz cavity also changes the vibration modes of the individual parts, all of which can cause differences in the calculation results.

In order to further analyze the sound insulation mechanism of the structure, we calculate the vibration modes and the sound field distribution of the structure at the sound insulation peaks, as shown in Fig.5. It is found that the plate and the mass on the top surface of the AHR form a local resonance and suppress the vibration of the frame and back plate when the first and second insulation peaks occur, thus impeding the propagation of the sound waves. We also calculate the elastic strain energy density distribution and the plane wave power consumption distribution, as shown in Fig.6. According to Fig.6, it is easy to find that the region of the high elastic strain energy shown in the lighter part is mainly concentrated in the edge region of the perforation where the mass and the thin plate are in contact, while the region of the high plane wave power consumption is mainly concentrated inside the perforation and near the neck. At the same time, the air in the Helmholtz cavity acts like a spring, causing the air in the neck to vibrate the back and the forth, which gradually dissipates the energy due to the friction between the air and the wall of the neck, thus attenuating the sound wave.

When a plane sound wave is incident vertically, the reflection and transmission coefficients can be calculated using $R = p_r/p_i$ and $T = p_t/p_i$, respectively, where p_i is the incident sound pressure, p_r

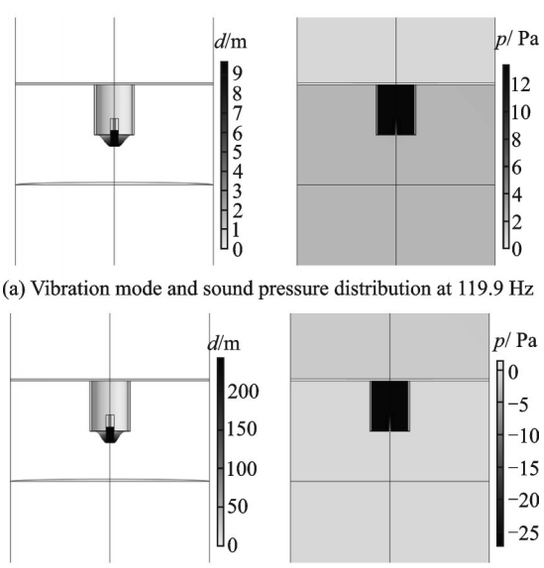

Fig.5 Vibration mode and sound pressure distribution at 119.9 Hz and 227.0 Hz

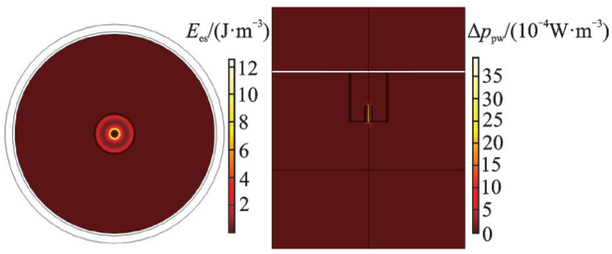

(a) Elastic strain energy density distribution and plane wave power consumption distribution at 119.9 Hz

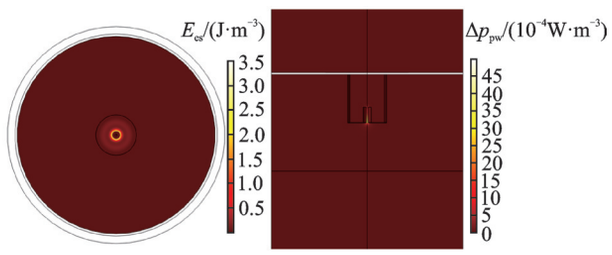

(b) Elastic strain energy density distribution and plane wave power consumption distribution at 227.0 Hz

Fig.6 Elastic strain energy density distribution and plane wave power consumption distribution at 119.9 Hz and 227.0 Hz

the reflected sound pressure, and p_t the transmitted sound pressure. The retrieval method can be used to calculate $\rho_{\_eff}/\rho_{\_air}$ and $K_{\_eff}/K_{\_air}$, as shown in Fig.7, where the black curve is the real part and the red curve the imaginary part. In terms of energy, the

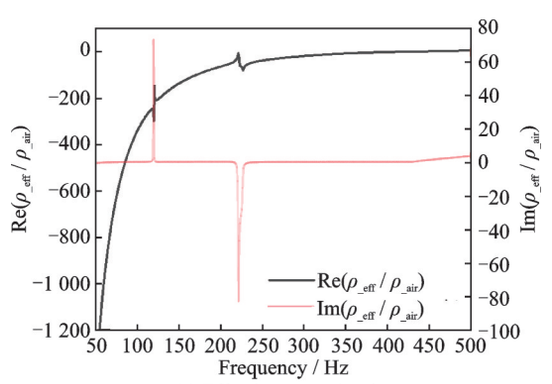

(a) Effective mass density

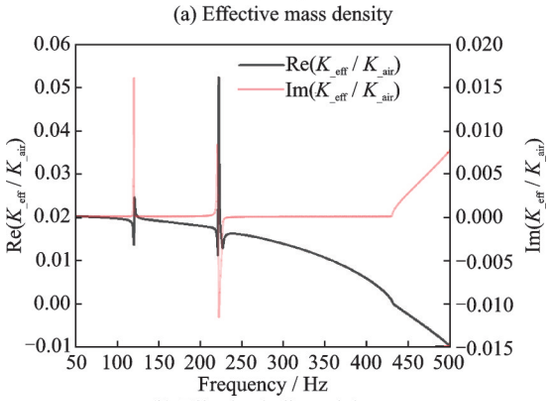

(b) Effective bulk modulus

Fig.7 Effective parameters of the structure

structure has the effect of absorbing the sound energy. When the resonance frequency reaches, the structure is driven by the sound energy to vibrate in anti-phase with the incident sound waves, achieving a negative effective mass density. Due to the strong resonance of the thin plate-mass structure, the air in the cavity absorbs less energy when the sound pressure changes in the Helmholtz cavity, so the effective bulk modulus significantly reduces but does not reach a negative value.

2 Effect of Structural Parameters on Sound Insulation Performance of AHR

From the previous analysis, it is clear that the length of the perforation, the radius of the perforation, the height of the space inside the cavity and the thickness of the plate will all change the resonant frequency of AHR, thus affecting the sound insulation performance of AHR. In order to achieve effective control of noise in specific frequency bands, we investigate the influence of structural parameters on the sound insulation performance of AHR by means of numerical simulations.

The effect of a single structural parameter on the sound insulation performance of AHR is investigated by varying the single structural parameter and fixing the remaining structural parameters. The AHR samples are attached to a 1 mm thick aluminium plate and the perforation length is adjusted by varying the height of the cylindrical mass. With varying the mass length, the sound transmission loss of AHRs with different perforation lengths is shown in Fig.8(a); the sound transmission loss of AHRs with different perforation radius is shown in Fig.8(b); the sound transmission loss of AHRs with different cavity heights is shown in Fig.8(c); the sound transmission loss of AHRs with different plate thicknesses is shown in Fig.8(d). According to Eq.(9), the resonant frequency of the Helmholtz cavity decreases as the perforation length increases, the perforation radius decreases and the cavity height increases. From Figs.8(a—c), the trend is consistent with Eq.(9). The frequencies at

insulation peaks decrease with the increase of the perforation length, increase with the increase of the perforation radius, and decrease with the increase of the cavity height. It also demonstrates that the first two peaks of AHR are related to the Helmholtz cavity and that the parameters of the Helmholtz cavity can be changed to adjust the work frequency of AHR. From Fig.8(b), we find that as the perforation radius increases, the increase in frequency at the first insulation peak significantly decreases compared with the second insulation peak. This is because the first insulation peak is more influenced by the resonance of the thin-plate mass structure, and the perforation radius significantly affects the equivalent stiffness of the thin plate-mass structure. As the perforation radius increases, the influence of the mass on the equivalent stiffness of the plate gradually decreases, thus the growth of resonant frequencies in plate-mass structure is gradually slowing down. However, from Fig.8(c), we find that the variation in cavity height has less effect on the frequency at the first insulation peak. This is because the variation in cavity height has very little effect on the resonance of the plate-mass structure, but still allows for significant adjustment of the frequency at the second insulation peak. According to Eqs.(1—6), the resonant frequency of the plate-mass structure increases as the thickness of the plate increases, which is consistent with the trend in Fig.8(d). The frequency at the first insulation peak significantly increases, demonstrating that the generation of the first insulation peak of AHR is closely related to the resonance of the plate-mass structure. The vibration of the plate-mass structure is influenced by the thickness of the plate, which in turn influences the motion of the air in the Helmholtz cavity and perforation, changing its resonant frequency.

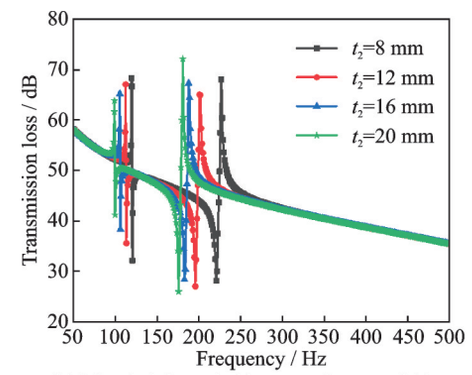

(a) Mass height varied between 8 mm and 20 mm

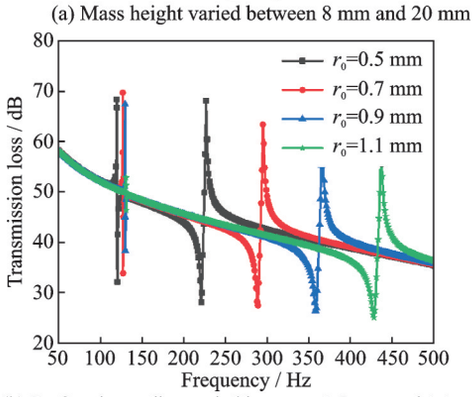

(b) Perforation radius varied between 0.5 mm and 1.1 mm

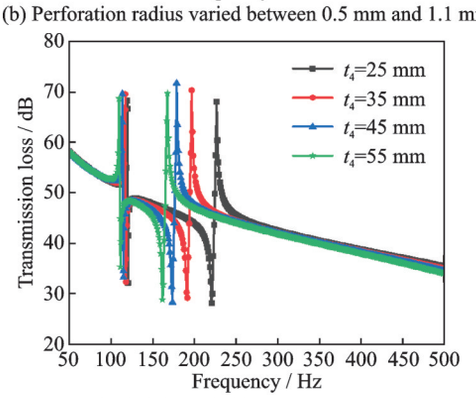

(c) Cavity height varied between 25 mm and 55 mm

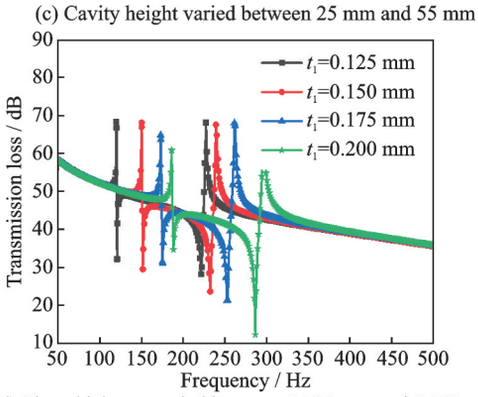

(d) Plate thickness varied between 0.125 mm and 0.200 mm

Fig.8 Transmission loss curves of the aluminium plates with AHRs for different perforation lengths, perforation radius, cavity heights and plate thicknesses

In summary, for attaching AHR to achieve the sound insulation, by increasing the perforation length, decreasing the perforation radius, increasing the cavity height and reducing the plate thickness, the frequency at the insulation peak can be reduced; conversely the frequency at the insulation peak will increase. It provides an important basis for the design of AHRs to control sound waves at specific frequencies.

3 Conclusions

We design a sub-wavelength sized attachable Helmholtz resonator with perforated thin-plate acoustic metamaterial on the top surface. Combined with the equivalent theoretical model, the change in sound insulation performance of samples after the application of AHR is investigated by numerical simulation. Firstly, the resonant frequencies of the various parts of AHR are predicted using an equivalent model, and the formation mechanism of the sound insulation peaks in the low-frequency range is analyzed in conjunction with the vibration modes and simulated fields. Then the effective parameters of AHR are calculated using the retrieval method and the link between the sound insulation peaks of AHR and the negative equivalent parameters are revealed. Finally, the influence of structural parameters on the sound insulation performance of AHR is investigated. The results show that by attaching AHR to the surface of the radiating structure, not only can the bending vibration of the structure be suppressed and the natural frequency of the structure be shifted towards the low-frequency range, but also at the ideal work frequency in the low-frequency range, causing local resonance for absorption of the sound energy and achieving a significant improvement in the sound insulation performance. The research and analysis of the structural parameters of AHR demonstrate that AHR can be designed for specific work frequencies depending on the radiation structure attached. This lightweight, sub-wavelength sized structure in the paper is a useful reference for the design of attachable acoustic metamaterials for low-frequency noise control.

References

[1] MULHOLLAND K A. Sound insulation at low frequencies[J]. Journal of the Acoustical Society of America, 1973, 54(4): 2734.

[2] LJUNGGREN S. Airborne sound insulation of thick walls[J]. Journal of the Acoustical Society of America, 1991, 89(5): 2338-2345.

[3] SHENG P, ZHANG X X, LIU Z, et al. Locally resonant sonic materials[J]. Physica B: Condensed Matter, 2000, 338(5485): 201-205.

[4] FANG N, XI D, XU J, et al. Ultrasonic metamaterials with negative modulus[J]. Nature Materials, 2006, 5(6): 452-456.

[5] DING Y, LIU Z, QIU C, et al. Metamaterial with simultaneously negative bulk modulus and mass density[J]. Physical Review Letters, 2007, 99(9): 093904.

[6] YANG Z, MEI J, YANG M, et al. Membrane-type acoustic metamaterial with negative dynamic mass[J]. Physical Review Letters, 2008, 101(20): 204301.

[7] LEE S H, PARK C M, SEO Y M, et al. Acoustic metamaterial with negative modulus[J]. Journal of Physics: Condensed Matter, 2009, 21(17): 175704.

[8] CHEN Y Y, HUANG G L. Analytical coupled vibro-acoustic modeling of membrane-type acoustic metamaterials: Membrane model[J]. The Journal of the Acoustical Society of America, 2014. DOI: 10.1121/1.4892870.

[9] SHENG P, MA G. Acoustic metamaterials: From local resonances to broad horizons[J]. Science Advances, 2016. DOI: 10.1126/sciadv.1501595.

[10] YONG L, ASSOUAR B M. Acoustic metasurface-based perfect absorber with deep subwavelength thickness[J]. Applied Physics Letters, 2016, 108(6): 204301.

[11] HUANG T Y, SHEN C, JING Y. Membrane- and plate-type acoustic metamaterials[J]. The Journal of the Acoustical Society of America, 2016, 139(6): 3240-3250.

[12] SHEN C, CUMMER S A. Harnessing multiple internal reflections to design highly absorptive acoustic metasurfaces[J]. Physical Review Applied, 2018, 9(5): 054009.

[13] KAI M, MARK A G, TIAN Q, et al. Holograms for acoustics[J]. Nature, 2016, 537: 518-522.

[14] ZHANG S, XIA C, FANG N. Broadband acoustic cloak for ultrasound waves[J]. Physical Review Letters, 2011. DOI: 10.1103/PhysRevLett.106.024301.

[15] MA G, YANG M, YANG Z, et al. Low-frequency narrow-band acoustic filter with large orifice[J]. Applied Physics Letters, 2013. DOI: 10.1063/1.4812974.

[16] LANGFELDT F, KEMSIES H, GLEINE W, et al. Perforated membrane-type acoustic metamaterials[J]. Physics Letters A, 2017, 381(16): 1457-1462.

[17] ZHOU R, WU W G, WEN Y F, et al. An acoustic metamaterial based on Helmholtz resonator with thin membrane[J]. Technical Acoustics, 2017, 36(4): 297-302.

[18] HE Z H, ZHAO J B, YAO H, et al. Sound insulation performance of Helmholtz cavity with thin film bottom[J]. Acta Physica Sinica, 2019, 68(21): 214302. (in Chinese)

[19] JIANG J L, YAO H, DU J, et al. Low frequency band gap characteristics of double-split Helmholtz lo-

cally resonant periodic structures[J]. Acta Physica Sinica, 2017, 66(6): 064301.

[20] FOKIN V, AMBATI M, CHENG S, et al. Method for retrieving effective properties of locally resonant acoustic metamaterials[J]. Physical Review B Condensed Matter, 2007, 76(14): 144302.

Authors Mr. **ZUO Hongwei** received the B.S. and M.S. degrees in engineering mechanics from Nanjing University of Aeronautics and Astronautics, Nanjing, China, in 2019 and 2022, respectively. His main research interests include vibration and acoustic properties of aerospace structures.

Dr. **SHEN Cheng** graduated in composite engineering from Harbin Institute of Technology, Harbin, China, in 2008, and received Ph.D. degree in solid mechanics from Xi'an Jiaotong University, Xi'an, China, in 2014. He is currently an associate professor in structural mechanics at the State Key Laboratory of Mechanics and Control of Mechanical Structures, Nanjing University of Aeronautics and Astronautics, Nanjing, China. His research interests include vibration and acoustic properties of aerospace structures.

Dr. **YANG Shasha** received the B.S. and Ph.D. degrees from Xi'an Jiaotong University, Xi'an, China, in 2008 and 2016, respectively. She is currently a lecturer in Nanjing Vocational University of Industry Technology, Nanjing, China. Her research interests include dynamic properties of intelligent materials and structures.

Author contributions Mr. **ZUO Hongwei** constructed the model, conducted the analysis, interpreted the results and wrote the manuscript. Dr. **LI Jinze** contributed to numerical analysis and helped perform the analysis with constructive discussions. Dr. **SHEN Cheng** supervised this study, polished English writing of the manuscript and contributed to the discussion and revision of the study. Dr. **YANG Shasha** reviewed the writing. Mr. **WANG Bin** contributed to the selection of materials with practical industrial experience. All authors commented on the manuscript draft and approved the submission.

Competing interests The authors declare no competing interests.

(Production Editor: XU Chengting)

一种基于贴附型Helmholtz共鸣器的声学超材料的隔声性能研究

左宏伟[1,2],李金泽[3],沈　承[1,2],杨莎莎[4],王　斌[5]

(1.南京航空航天大学机械结构力学及控制国家重点实验室,南京 210016,中国;
2.南京航空航天大学多功能轻量化材料与结构工信部重点实验室,南京 210016,中国;
3.香港理工大学机械工程系,香港 999077,中国;
4.南京工业职业技术大学机械工程学院,南京 210023,中国;
5.苏州顶裕节能设备有限公司,苏州 215213,中国)

摘要:针对低频噪声的控制问题,提出了一种新的穿孔薄板声学超材料,其具有可贴附的Helmholtz共鸣器(Attachable Helmholtz resonator,AHR),底面可以直接贴附在需要抑制声辐射的结构上。通过使用有限元方法研究了贴附AHR的铝板在垂直入射的平面波下的声传输损失。研究结果表明,AHR在50~500 Hz频段内隔声表现良好,出现了2个新的隔声峰。首个新隔声峰值对应的频率降至了120 Hz左右。研究板厚、腔深、穿孔半径和穿孔长度对超材料隔声性能的影响,证明可以通过改变结构的声辐射特性,实现对特定频率声辐射的有效抑制。

关键词:Helmholtz共鸣器;声学超材料;传声损失